Journal of Power Sources 236 (2013) 215–223

Contents lists available at SciVerse ScienceDirect

Journal of Power Sources

journal homepage: www.elsevier.com/locate/jpowsour

Copper nanocrystal modified activated carbon for supercapacitors with enhanced volumetric energy and power density

Lili Zhang [a,b], Stephanie L. Candelaria [b], Jianjun Tian [b], Yanwei Li [b], Yun-xia Huang [b], Guozhong Cao [b,*]

[a] Jiangsu Key Laboratory for Chemistry of Low-Dimensional Materials, Huaiyin Normal University, Huai'an, Jiangsu Province 223300, PR China
[b] Department of Materials Science and Engineering, University of Washington, Seattle 98195, USA

HIGHLIGHTS

- Cu modified activated carbon for supercapacitor was synthesized by *in situ* solution-based absorption–reduction method.
- The incorporation of copper nanocrystals in AC has little effect on the surface area and porosity of activated carbon.
- The incorporation of copper nanocrystals improves the electrical conductivity of the carbon network.
- The addition of Cu can greatly increase the volumetric capacitance and power density of AC.
- The effects of copper content on the electrochemical properties of AC were investigated.

ARTICLE INFO

Article history:
Received 16 November 2012
Received in revised form
10 January 2013
Accepted 13 February 2013
Available online 4 March 2013

Keywords:
Supercapacitor
Copper
Volumetric capacitance
Activated carbon

ABSTRACT

Copper nanocrystals homogeneously dispersed in activated carbon (AC) were synthesized by an *in situ* solution-based absorption–reduction method, and the resulting composites were characterized and studied for supercapacitor application. The effects of copper nanocrystals and their content on the electrochemical properties of the obtained AC composites were investigated using multiple techniques, including X-ray photoelectron spectroscopy, nitrogen sorption analysis, cyclic voltammetry, galvanic cycling, and electrochemical impedance spectroscopy. Results showed that the addition of copper nanocrystals in the AC composites has little effect on the surface area and porosity of AC, and is helpful to reduce its equivalent series resistance, which is favorable to achieve higher charge/discharge rate and improve its power density when used as electrodes for supercapacitors. Copper nanocrystals and the partially oxidized phase CuO act as pseudo-active materials and improve the capacity of the AC composite electrode. The volumetric capacity, energy density, and power density of copper nanocrystal modified activated carbon are much higher than those of AC and AC mechanically mixed with copper particles. Copper nanocrystal modified AC presents a high volumetric capacitance of 62 F cm^{-3}, more than twice of that of unmodified AC.

1. Introduction

Currently, electric double layer capacitors (EDLCs) have evoked wide interest in recent years due to their ability to supply high power in short-term pulses, which makes them very good energy storage devices for applications such as hybrid power sources for electric vehicles and portable electronic devices [1–4]. The working mechanism of EDLCs is based on the quick formation of a double layer of surface charges and counter-ions at the electrode/electrolyte interface. For the attainment of high capacity and fast kinetics, electrode materials for EDLCs should have large surface area to accumulate a large amount of charges, and a size-controlled porous channel system for easy access of the electrolyte [1,3]. A lot of efforts have been devoted to develop highly porous electrodes with very high specific surface area and low density. These electrode materials offer high gravimetric energy and power densities; however, the volumetric energy and power densities are typically very low.

So far, activated carbons (AC) are the mostly widely used EDLC electrode materials due to their large surface area, relatively good electrical properties, moderate cost, and somewhat controllable pore size [1–7]. However, despite the high specific surface area, application of porous carbon materials has been limited due to their low conductivity and incomplete use of all

* Corresponding author. Tel.: +1 206 616 9084; fax: +1 206 543 3100.
E-mail address: gzcao@u.washington.edu (G. Cao).

0378-7753/$ – see front matter © 2013 Elsevier B.V. All rights reserved.
http://dx.doi.org/10.1016/j.jpowsour.2013.02.036

pores for charge accumulation. For AC, typically only about 10–20% of the "theoretical" capacitance was observed due to the presence of micropores that are inaccessible to the electrolyte, wetting deficiencies of electrolytes on electrode surface, and/or the inability of a double layer to form successfully in the pores [8]. Several methods have been used to control the microstructure of porous carbon, but these techniques are onerous and expensive [2,7–9].

Introducing pseudocapacitance to traditional EDLCs can significantly increase their capacitance. This involves voltage dependent faradaic reactions between the electrode and the electrolyte, either in the form of surface adsorption/desorption of ions, redox reactions with the electrolyte, or doping/undoping of the electrode materials [1–4]. The most commonly studied materials include those with oxygen- and nitrogen-containing surface functional groups, electrically conducting polymers, such as polyanilines [1–4,10] and polypyrrole [1–4,11,12], transition metal oxides e.g., RuO_2, MnO_x, SnO_2, NiO, CuO, etc. [4,13–20], or the combination of conductive polymers and transition metal oxides [4,21]. Incorporating metal onto the surface of porous carbon can work to improve its conductivity due to electronic interactions between the two components [20]. One metal that is of particular interest is copper, which is an excellent conductor, low cost, abundant, and nontoxic. Previous studies [22,23] have shown that introducing copper to mesoporous activated carbons can significantly enhance the capacitance of an electrochemical capacitor. Hwang and Teng reported that electrodeposition of copper on activated carbon fabric can provide a simple and economical means to substantially enhance the capacitance of carbonaceous electrodes [22]. Men et al. achieved high capacitance using a doping method to fabricate Cu-doped activated carbon composites from phenolic resins [23]. In this study, we attempt to introduce copper nanocrystals both on the surface and in the pores of activated carbon; modification can increase the accessible surface area, improve the wettability of the electrolyte, and reduce the electrical resistance. In addition, copper nanocrystals act as a pseudo-active material and add faradaic capacitance to the EDLCs, similar to noble metals such as Pt and Pd [4], but much more economic. All these factors will result in a greatly enhanced active material in a given volume and, thus, significantly improve its volumetric capacity, energy density, and power density.

Microsized copper particles directly admixed with AC are difficult to incorporate uniformly, and can cause a decrease the surface area and porosity of AC. Therefore, in this paper, copper nanocrystals deposited directly on the surface and inside pores of AC were synthesized by an *in situ* solution-based absorption–reduction method. Fig. 1 illustrates the rationale and intended structure of the AC–Cu nanocomposites. Using the *in situ* solution-based absorption–reduction technique, copper nanocrystals with small size and high dispersibility were deposited directly onto the surface and inside the pores of AC. The microstructures and electrochemical properties of the resultant AC–Cu nanocomposites were systematically studied with particular focus devoted to the effects of the copper content on the electrochemical properties of the AC composites.

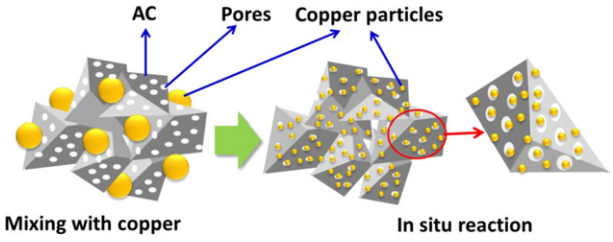

Fig. 1. Schematic illustration estimated structure of AC–Cu composites.

2. Experimental section

2.1. Materials synthesis

AC–Cu composites were synthesized by an *in situ* absorption–reduction method. In order to improve the reactive activity, especially the absorbing ability of activated carbon (AC Calgon), the AC was first acid treated with HNO_3. 5 g of AC was refluxed in 50 mL 6 M HNO_3 solution while stirring for 1 h at 80 °C to introduce negative groups onto its surface. The obtained product was labeled as AC–H. Then 0.34 g AC–H and a given amount of $CuCl_2 \cdot 2H_2O$ were ultrasonically dispersed in 12 mL distilled water. After ultrasonication for 10 min, the mixture solution was kept stirring at room temperature for 2 h, and then filtered and washed with distilled water 3 times to eliminate Cl^-. Finally, the powder was sintered at 450 °C for 2 h in a nitrogen atmosphere. As an example, 0.0908 g $CuCl_2 \cdot 2H_2O$ was dissolved in 12 mL distilled water; then 0.3381 g AC–H was dispersed in the aforementioned $CuCl_2$ solution. After ultrasonicating, stirring, and heat treating in N_2, the product was noted as AC–Cu (8%). Similarly, AC–Cu (4%), AC–Cu (12%), and AC–Cu (16%) were also synthesized.

For comparison, activated carbon was mechanically mixed with copper powder (with a Cu% of 12%) and the mixture was denoted as AC–Cu-mix (12%). This was used as the reference for XRD, SEM, nitrogen sorption, and electrochemical analysis.

2.2. Materials characterization

The surface morphology of AC and the AC–Cu composites was observed using scanning electron microscopy (SEM-7000) and phase and crystallite size were studied using X-ray diffraction (XRD, Philips 1820X-Ray Diffractometer). X-ray photoelectron spectroscopy (XPS) is used to determine the atomic composition of the AC composites. Spectra are taken on a Surface Science Instruments S-probe spectrometer. Data analysis is carried out using the Service Physics ESCA2000-Analysis program (Service Physics, Bend, OR). Nitrogen sorption isotherms and the porous structure are measured using a Quantachrome NOVA 4200e. Samples are degassed at 250 °C under vacuum for at least 6 h prior to measurement.

2.3. Electrochemical analysis

Electrodes for electrochemical measurements are prepared from active materials according to reference [24]. The electrode was formed by mixing 85 wt% active material, 10 wt% acetylene black, and 5 wt% PTFE. The mixture is rolled into sheets with a thickness of 0.07–0.08 mm and electrodes are punched out with a diameter of 10 mm. A Celgard porous film separates the electrodes and specially coated aluminum contacts are used to reduce the interfacial effect. The electrolyte used is tetraethylammonium tetrafluoroborate (TEATFB) in saturated 50–50 propylene carbonate–dimethylcarbonate. The electrode assembly is placed in a flat cell and electrolyte is added in an argon-rich environment. The samples were placed under vacuum to increase the penetration of the electrolyte into the pores.

Cyclic voltammograms (CV) and galvanic cycles (GC) are taken using a Solartron 1287A with a voltage range between 0 and 2 V. The CVs are measured at scan rates of 100, 50, and 10 mV s^{-1}, and the GCs at 2, 1, 0.2, and 0.1 A g^{-1}. Electrochemical impedance spectroscopy is performed using the Solartron 1287A in conjunction with a Solartron 1260FRA/impedance analyzer. Analog controller voltage amplitude of 10 mV and a frequency range of 0.05 Hz–1 MHz is used for this scan.

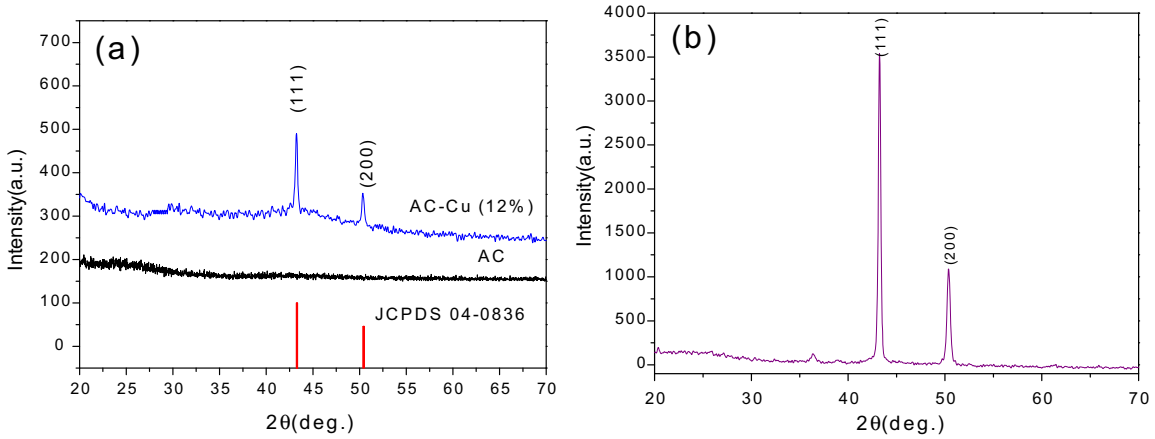

Fig. 2. XRD patterns of (a) AC, (b) copper nanocrystals modified AC (with 12 wt% Cu), and (c) mechanically mixed AC and copper powder (with 12 wt% Cu).

3. Results and discussion

3.1. Composition and structure

In order to understand the structure and the difference between the samples obtained by the *in situ* technique and mechanical mixing method, AC, AC–Cu (12%) and AC–Cu-mix (12%) were chosen as models to undergo the following characterization.

To determine the existing state of copper in the AC–Cu (12%) composite, XRD patterns of AC–Cu-mix and AC are presented in Fig. 2. It can be seen that AC is noncrystalline. After Cu modification (Fig. 2a), the peaks corresponding to Cu (111) and (200) were observed (JCPDS 04-0836), which came from the reduction of Cu^{2+} by the reductive group on the surface of activated carbon [21]. On the other hand, the AC–Cu composite (Fig. 2a) shows broader peaks and lower intensity than that of AC–Cu-mix (Fig. 2b), suggesting that the AC–Cu composite is composed of small Cu particles with relatively low crystallization [25]. Based on the Scherrer equation, the crystalline size of AC–Cu-mix and the AC–Cu composite is 580 nm and 15 nm, respectively. This result will be confirmed later by SEM results.

The presence of copper in AC–Cu composites was further identified by X-ray photoelectron spectroscopy (XPS). Fig. 3 gives the full spectrum of the AC–Cu composites, which exhibited the peaks of C, O, and Cu. The wt% of C, O, and Cu are listed in Table 1. While it can be seen that the actual content of Cu in the AC–Cu composites is lower than the initial dosage for all samples, the content does increase with the increasing dosage of Cu^{2+}. Since XPS is a surface technique, it is possible that there is a greater concentration of Cu particles immerged within the interior pores of AC that cannot be detected by XPS. Regardless, the presence of copper nanocrystals in AC is thought to be helpful to improve the conductivity.

From the inset spectrum of Cu2p shown in Fig. 3a, the characteristic shake-up peak of Cu^{2+} $2p_{3/2}$ appeared. This indicates the existence of Cu^{2+}, which is caused by the oxidation of the exterior

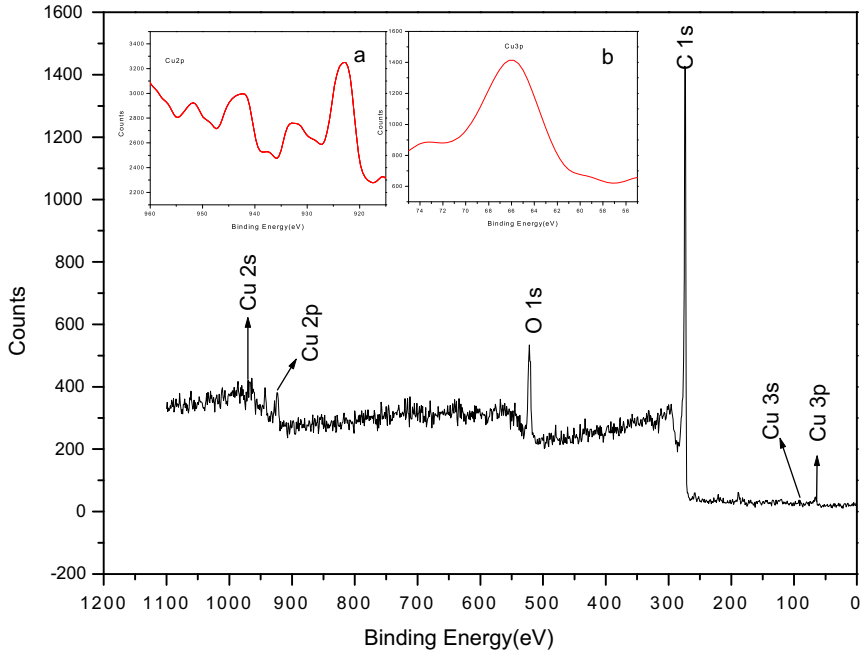

Fig. 3. Full XPS spectra of AC–Cu (12%), with detailed peaks for (a) Cu^{2+} $2p_{3/2}$ and (b) Cu 3p.

Table 1
Wt% of C, O, and Cu from XPS in the AC–Cu composites.

Sample	AC–Cu (4%)	AC–Cu (8%)	AC–Cu (12%)	AC–Cu (16%)
C%	91.40	89.16	87.15	83.59
O%	6.05	7.69	7.06	9.19
Cu%	2.56	3.16	5.79	8.22

Cu^0 in the AC–Cu composite. The existing form of Cu^{2+} is CuO since its binding energy is close to 933.5 eV, which is similar to the reference [25]. Results indicate that copper exists in the Cu^0–Cu^{2+} mixed state but with Cu^0 dominating. This partial oxidation of Cu may induce faradaic capacitance that adds to the capacitance of the EDLCs.

Fig. 4 shows the SEM morphologies of AC–Cu-mix and the AC–Cu composites. From Fig. 4a and b, it can be seen that the spherical Cu particles with sizes of 1–2 μm were distributed non-uniformly in the middle of the block-like AC. Meanwhile in Fig. 4c, copper nanocrystals cannot be easily detected under lower magnification. In Fig. 4d, it can be seen that copper nanocrystals with high dispersibility and uniform size of about 10–30 nm are directly grown onto the surface of AC (Fig. 4d inset), since the surface energy of Cu is much larger than that of carbon [26]. There are also some Cu nanoparticles observed on the surface of the cross-section, implying some Cu nanoparticles are inside the pores of AC.

Fig. 5b and c is the energy dispersive X-ray spectroscopy (EDS) distribution maps of Cu and C from the surface and cross-section of AC–Cu composites in Fig. 5a. The concentration of Cu and C elements on the surface of AC is higher than that in the cross-section due to the distance between EDS probe and scan area. However, Fig. 5b and c shows that the distribution of Cu is similar to that of C. This indicates that Cu not only exists on the surface of AC, but also permeates into the pores of AC. During synthesis of the AC–Cu composites, AC was first immersed in the $CuCl_2$ precursor solution. Therefore, some copper ions entered into the inner pores and were reduced in the subsequent heat treatment process. This causes the copper crystals to distribute uniformly from the surface to the inner pores of AC. As for the big particles of copper concentrated on the surface (Fig. 4c and d), this is possibly caused by the Cu nucleus on the surface of AC growing quickly during precursor reduction in the heat treatment process. However, the growth of the nucleus is restrained by the pore space, so the size of Cu on the AC surface is much larger than that in the inner pores.

The nitrogen adsorption–desorption isotherms of AC, the AC–Cu composite, and AC–Cu-mix were used to determine how the surface area, pore volume, and pore diameter change after modification. Isotherms and pore size distribution curves are shown in Fig. 6 and the corresponding data are presented in Table 2. It can be seen that the isotherm profiles (Fig. 6a) are similar and can be classified as type IV according to the IUPAC classification [27]. Comparing with the unmodified AC, the specific surface area and pore volume of the AC–Cu composite synthesized by the *in situ* reaction increased slightly because many Cu nanocrystals were loaded onto the surface of AC, which may result in the formation of some new quasi pores or poles (Table 2 and Fig. 6b). As for the pore diameter (Fig. 6b), it decreased after modification since some Cu crystals immersed into the pores of AC. This small change indicates that the addition of Cu will not deteriorate the formation of a double layer of charges at the electrode/electrolyte interface. Instead, it will help speed up this process. On the other hand, AC–Cu-mix presents lower surface area and smaller pore volume and pore diameter. Based on the literature, all these differences will have great effects on the electrochemical properties [1–8].

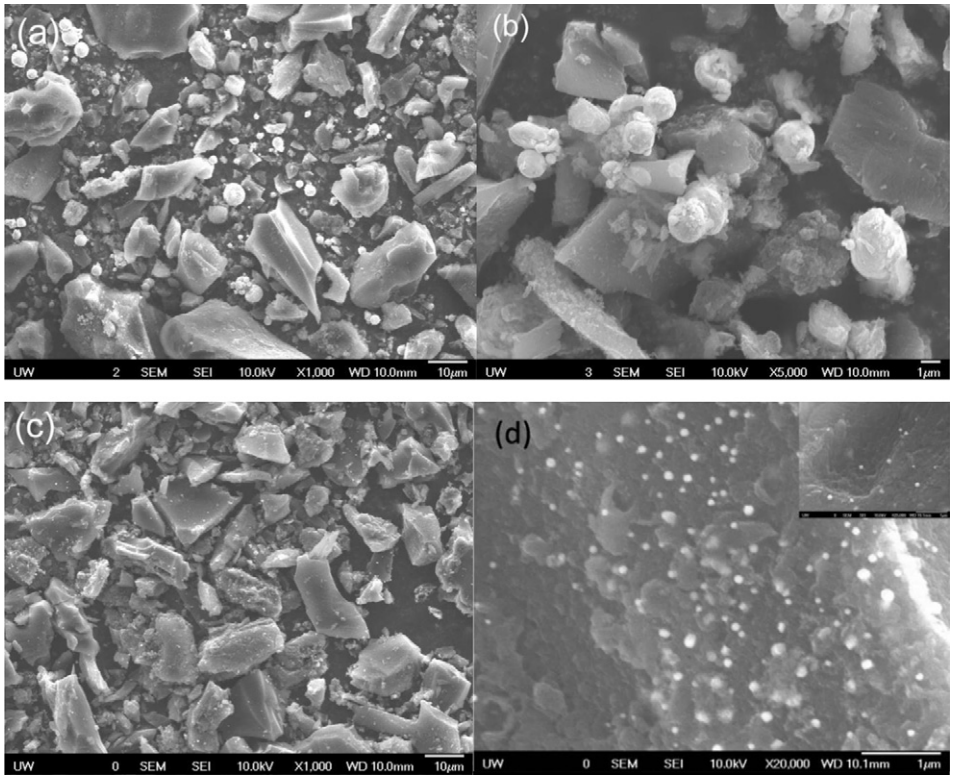

Fig. 4. SEM images of AC–Cu mix (12%) (a) (b) and AC–Cu(12%) (c) (d) under different magnification.

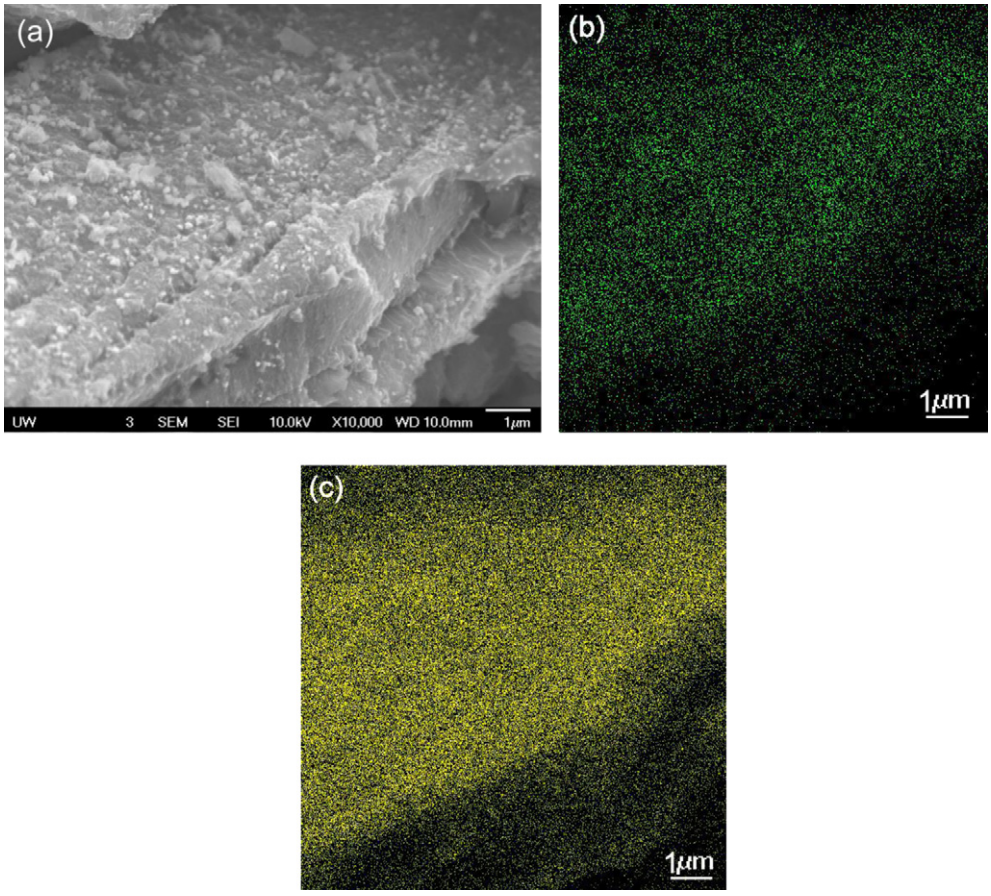

Fig. 5. (a) SEM image and EDS distribution maps of (b) Cu and (c) C in AC–Cu (12%).

3.2. Electrochemical properties

Fig. 7 presents the supercapacitive properties of the AC–Cu (12%) composite. In Fig. 7a, it can be seen that the cyclic voltammograms (CV) have a nearly rectangular shape from 10 mV s^{-1} to 100 mV s^{-1}, which indicates quick charge propagation in this material. The shape remains almost the same after 50 cycles, indicating only a slight decrease in capacitance, even at 100 mV s^{-1} (Fig. 7b). The galvanostatic charge/discharge curves (GC) at different current densities (Fig. 7c) are fairly symmetric and exhibit the linear charging behavior characteristic of electric double layer capacitance. However, the discharge time decreases with the increased applied current. Fig. 7d shows the variation in the capacitance retention at 0.2 A g^{-1} as function of the cycle number. It can be seen that the capacitance remains at approximately 78 F g^{-1} and decreases only slightly for the AC–Cu (12%) composite, indicating a supercapacitor made from this material presents good stability and maintains 98.8% capacitance after 100 cycles, which is consistent with the CVs.

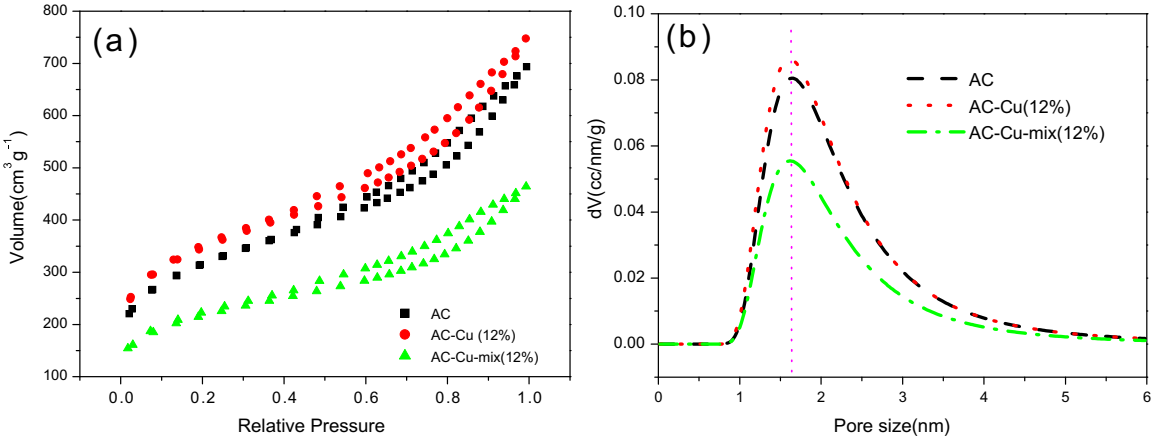

Fig. 6. (a) Nitrogen sorption isotherms for AC, AC–Cu (12%) and AC–Cu-mix (12%) and (b) micropore size distributions.

Table 2
Surface areas, pore volumes, and pore diameters of AC, AC–Cu (12%) and AC–Cu-mix (12%).

Sample	Surface area ($m^2\ g^{-1}$)			Pore volume ($cm^3\ g^{-1}$)		Pore diameter (nm)	
	Total	Mesopores	Micropores	Mesopores	Micropores	Mesopores	Micropores
AC	1021.3	301.3	445.8	0.663	0.241	3.19	1.64
AC–Cu	1108.0	319.2	540.2	0.727	0.296	3.18	1.62
AC–Cu-mix	693.6	187.2	332.0	0.430	0.180	3.18	1.52

Comparatively, the cyclic properties and capacity of AC–Cu-mix (12%) were quite different (Fig. 8). In the CV curves, the fairly rectangular shape of the first cycle indicates the capacitive behavior of an electric double layer, but it begins to shrink at high voltage with an increase in cycles, indicating the obvious decay of the electrode materials. Based on its GC curve, the charge and discharge capacity is quite small. This phenomenon may be due to the corruption of Cu particles because of its poor dispersibility and the infinitesimal interaction with AC.

Fig. 9 shows the CV and GC curves for all the AC–Cu composites with different copper content. It can be seen that the voltammograms maintained the rectangular shape with 4% Cu. In the CV curve of AC–Cu (8%), the ideal rectangular shape began to distort. With the increasing content of Cu, the distortion becomes obvious. When the content of Cu increased to 12%, a pair of weak oxidation–reduction peaks appeared, and when it reached 16%, an obvious pair of oxidation–reduction peaks was observed. This indicates faradaic capacitance exists in addition to the typical double-layer capacitance, and the contribution from faradaic capacitance increases with the increase of Cu content. Although the exact mechanism of this phenomenon is not known, it might be attributable to the reversible adsorption of electrolyte ions onto the surface of Cu nanocrystals in the AC–Cu composites, similar to that reported in literature on the surface of noble metals, such as platinum or gold [4]. The mixed states of Cu^0–Cu^{2+} may add electrochemical reactions during the charge/discharge process. The oxidation and reduction peaks are close to each other, suggesting good reversible charge and discharge ability. Therefore, by adding this pseudocapacitive process, the capacitance of the AC–Cu composite will increase. Fig. 9b shows the first charge–discharge GCs measured at the same current density of 0.2 A g^{-1}. When the content of Cu is between 4 and 8%, the samples exhibit linear charging behavior, while AC–Cu (12%) and AC–Cu (16%) composites present non-linear charging behavior characteristic of pseudocapacitive reactions, which is consistent with the CV curves.

When expanding the scale of GC curves (Fig. 9c), it can be seen that the IR-drop is different for each of the AC–Cu composites, and the sequence is as follows: AC–Cu (16%) > AC–Cu (12%) > AC > AC–Cu (8%) > AC–Cu (4%). The calculated resistances are listed in Table 3. AC–Cu (16%) presented the largest resistance, whereas AC–

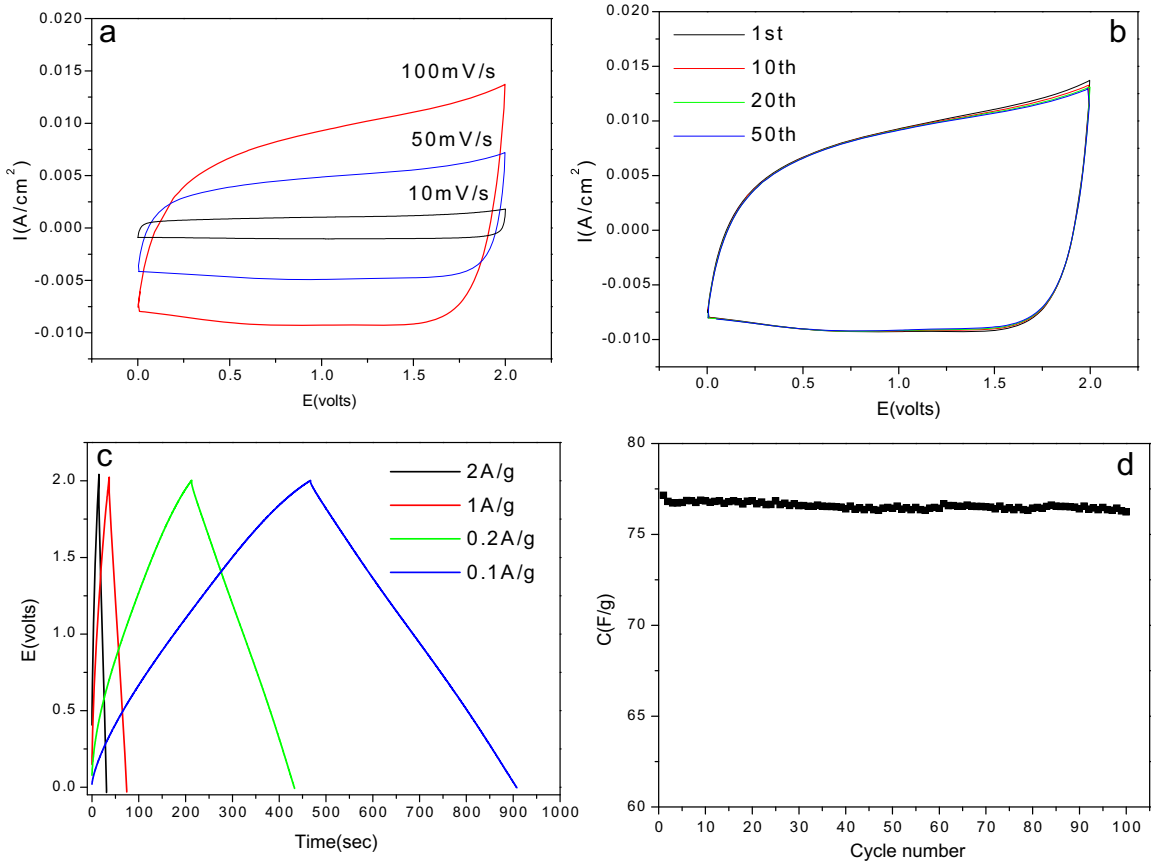

Fig. 7. Supercapacitive properties of AC–Cu (12%): (a) CV curves at different scan speeds, (b) CV curves for different cycles taken at 100 mV s^{-1}, (c) Galvanostatic charge/discharge curves at different current densities, (d) variation in the capacitance retention (0.2 A g^{-1}) as a function of the cycle number.

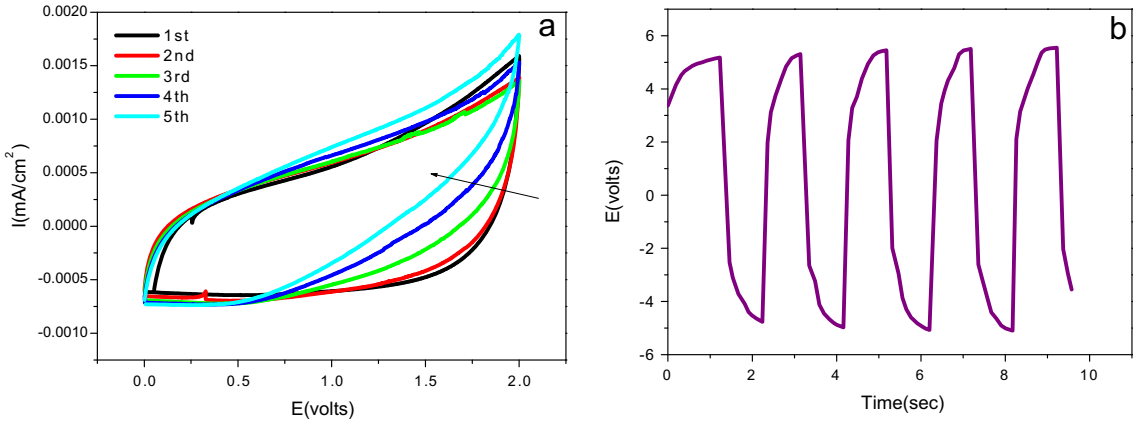

Fig. 8. (a) CV (10 mV s^{-1}) and (b) GC (0.2 A g^{-1}) curves for AC–Cu-mix (12%).

Cu (4%) emerged as the smallest. The resistance will affect the supercapacitive properties of the material, including energy and power density.

The specific capacitance, volumetric capacitance, energy density, and power density were calculated from the discharge slopes of the GC curves and the results are shown in Table 4. It can be seen that the specific capacitance increased slightly with the introduction and increasing amount of copper nanoparticles, but the volumetric capacity, energy density, and power density increased significantly. These improvements can be ascribed to the following reasons: first, with Cu nanocrystal modification, the pore structure was tuned and made more accessible for the electrolyte ions to travel within the electrodes, which resulted in the improvement of the charge/discharge rate. Second, the absorption/desorption of the electrolyte ions onto the surface of the Cu nanocrystals and the mixed state of Cu^0–Cu^{2+} may add to the capacitance through

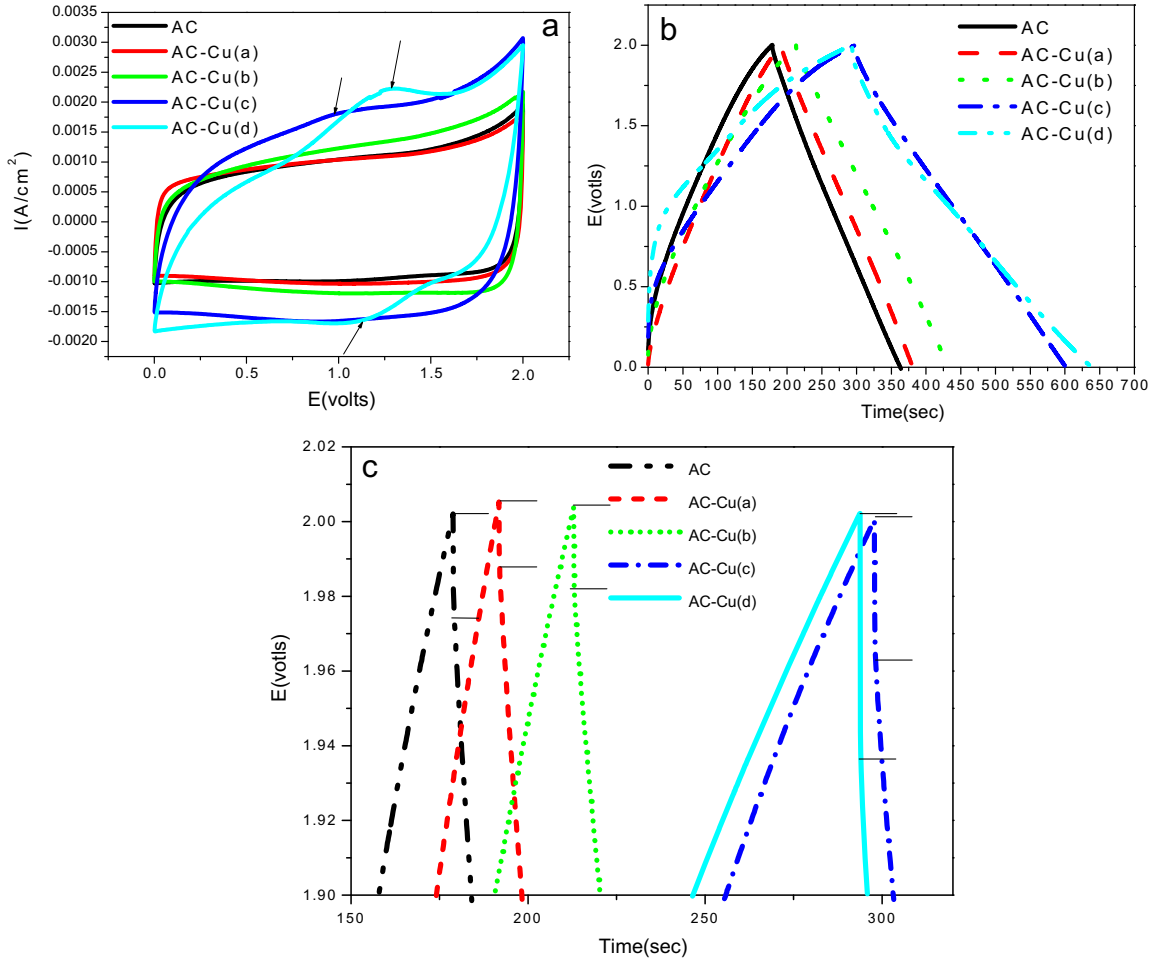

Fig. 9. (a) CV (scan rate 10 mV s^{-1}) and (b) GC (charge/discharge rate at 0.2 A g^{-1}) curves of AC–Cu composites with different copper contents: 4% (a), 8% (b), 12% (c), and 16%(d).

Table 3
Resistance of the electrodes calculated based on the GC IR-drop (R) and read from Nyquist plot (R_S) of AC–Cu composites with different content of copper.

Sample	AC	AC–Cu (4%)	AC–Cu (8%)	AC–Cu (12%)	AC–Cu (16%)
R (Ω)	18	12	15	22	34
R_S (Ω)	10.4	7.0	8.0	12.3	16.8

pseudocapacitive and electrochemical reactions. Since Cu is more massive than carbon and the specific capacitance is based on F g^{-1}, the specific capacitance of the AC–Cu composite does not increase obviously. But when the capacitance is normalized per unit volume, this increase becomes notable owing to the more compact structure, showing obvious merits in potential applications for low-volume high-capacitance devices [6].

From Table 4, it also can be seen that the specific and volumetric capacitance, energy density, and power density of AC–Cu composites increased with the initial increase of copper content (below 12%), and then decreased with the further increase of copper content. Excessive copper may have resulted in the reduction of pore size and the pore accessibility.

Fig. 10 shows the Nyquist plot for the AC–Cu composites measured by electrochemical impedance spectroscopy (EIS). At the high frequency region, the semicircle signifies the charge transfer process at the electrode–electrolyte interface. This can be suitably modeled as a double-layer capacitor in parallel with charge-transfer resistor [28]. The equivalent series resistance (R_S) for each sample is read from Nyquist plots and listed in Table 3. AC–Cu (4%) exhibits the lowest equivalent series resistance (7.0 Ω), and AC–Cu (12%) has a smaller resistance (12.3 Ω) than AC (10.4 Ω), while AC–Cu (16%) has the largest resistance (16.8 Ω). This trend is consistent with the IR-drop for each sample seen in the GC curves. The differences in equivalent series resistance can be attributed to two mechanisms: one is that the Cu in the AC–Cu composites is useful for improving the conductivity of the electrode material; the other is that Cu nanocrystals block the entrance of the pores in the carbon, which may be harmful to charge transfer and lead to high resistance. When these two factors are balanced, the composites will have the best electrochemical properties, and the highest capacitance and power density will be obtained. Therefore, appropriate amounts of Cu nanocrystals deposited in the channels of activated carbon may improve the supercapacitor charge/discharge rate, but too many Cu nanocrystals may decrease the charge/discharge rate. The lower frequency region of the Nyquist plots is representative of ion diffusion in the electrode structure, and a completely vertical slope indicates pure capacitive behavior. The more vertical the curve, the more closely the supercapacitor behaves as an ideal capacitor. Therefore, the AC–Cu (4%) and AC–Cu (12%) present better capacitive behavior than AC. But when combined with the charge/discharge ability, AC–Cu (12%) should be chosen as the best electrode material for supercapacitors.

Table 4
Specific and volumetric capacitance, energy density, and power density of AC–Cu composites based on mass, volume, R_S, and current density (0.2 A g^{-1}).

Sample	Gravimetric			Volumetric		
	C (F g^{-1})	E (Wh kg^{-1})	P (kW kg^{-1})	C (F cm^{-3})	E (Wh cm^{-3})	P (kW cm^{-3})
AC	64.6	34.1	17.3	30.4	17.1	8.5
AC–Cu (4%)	77.0	43.4	29.7	46.2	26.0	16.3
AC–Cu (8%)	76.5	44.0	32.1	53.3	30.0	19.3
AC–Cu (12%)	78.9	43.9	27.1	62.2	34.7	18.9
AC–Cu (16%)	74.0	41.4	15.3	60.1	33.6	10.3

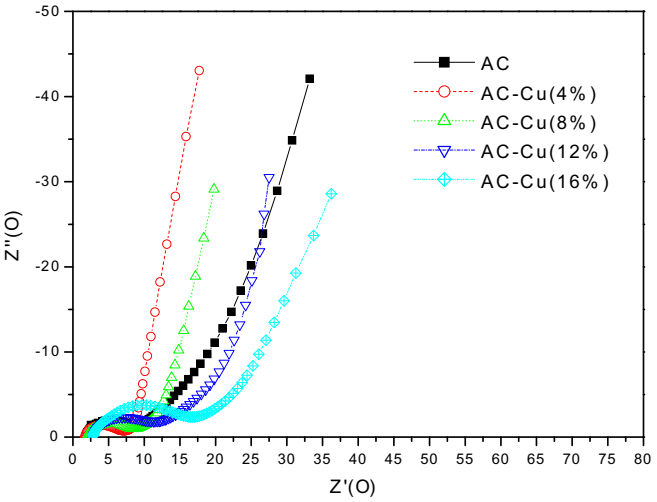

Fig. 10. Nyquist plot of AC–Cu composites with different copper content.

4. Conclusion

Modification of activated carbon with copper nanocrystals, both on the surface and in the internal pore surface of the carbon, has proved to increase the capacitive behavior for supercapacitor applications, especially for the improvement of volumetric capacity. The Cu nanocrystals tuned the porous structure of carbon to match the size of the electrolyte ions and induced faradaic reactions, which contribute to the capacitance that is already present from electric double-layer formation. Additionally, the partial oxidation of Cu to CuO helps improve the electrical conductivity in a way that benefits the system. The effects of copper content on the electrochemical properties of AC were investigated. In order to achieve higher capacity, energy density, and power density, the dosage of Cu in AC composite of 12%, resulting in the highest specific and volumetric capacity at 79 F g^{-1} and 62 F cm^{-3}, respectively.

Acknowledgments

This work is supported in part by National Science Foundation (DMR-0605159 and CMMI-1030048) and Intel Corporation. Lili Zhang would like to acknowledge the Program for Jiangsu Higher Institutions Key Basic Research Projects of Natural Science (10KJA430005), Technological Research Foundation of Huai'an City (HAG2011008) and Qing Lan Project for financial support.

References

[1] S.L. Candelaria, Y.Y. Shao, W. Zhou, X.L. Li, J. Xiao, J.G. Zhang, Y. Wang, J. Liu, J.H. Li, G.Z. Cao, Nano Energy 1 (2012) 195–220.
[2] S.L. Candelaria, R. Chen, Y.H. Jeong, G.Z. Cao, Energy Environ. Sci. 5 (2012) 5619–5637.
[3] L.L. Zhang, X.S. Zhao, Chem. Soc. Rev. 38 (2009) 2520–2531.
[4] G.P. Wang, L. Zhang, J.J. Zhang, Chem. Soc. Rev. 41 (2012) 797–828.
[5] Y.P. Zhai, Y.Q. Dou, D.Y. Zhao, P.F. Fulvio, R.T. Mayes, S. Dai, Adv. Mater. 23 (42) (2011) 4828–4850.
[6] Y.W. Zhu, S. Murali, M.D. Stoller, K.J. Ganesh, W.W. Cai, et al., Science 332 (2011) 1537–1541.
[7] J. Chmiola, G. Yushin, Y. Gogotsi, C. Portet, P. Simon, P.L. Taberna, Science 313 (2006) 1760–1763.
[8] M. Anouti, L. Timperman, Mostafa el hilali, A. Boisset, H. Galiano, J. Phys. Chem. C 116 (2012) 9412–9418.
[9] Y. Gogotsi, A. Nikitin, H.Y. Ye, W. Zhou, J.E. Fischer, B. Yi, C. Henry, Nat. Mater. 2 (2003) 591–594.
[10] J.J. Xu, K. Wang, S.Z. Zu, B.H. Han, Z.X. Wei, ACS Nano 4 (9) (2010) 5019–5026.

[11] A. Davies, P. Audette, B. Farrow, F. Hassan, Z.W. Chen, J.Y. Choi, A.P. Yu, J. Phys. Chem. C 115 (2011) 17612–17620.
[12] S. Biswas, L.T. Drzal, Chem. Mater. 22 (20) (2010) 5667–5671.
[13] J.F. Zang, S.J. Bao, C.M. Li, H.J. Bian, et al., J. Phys. Chem. C 112 (2008) 14843–14847.
[14] H.C. Gao, F. Xiao, C.B. Ching, H.W. Duan, ACS Appl. Mater. Interfaces 4 (2012) 2801–2810.
[15] D.L. Yan, Z.L. Guo, G.S. Zhu, Z.Z. Yu, H.R. Xu, A.B. Yu, J. Power Source 199 (2012) 409–412.
[16] Z.B. Lei, F.H. Shi, L. Lu, ACS Appl. Mater. Interfaces 4 (2012) 1058–1064.
[17] H.X. Zhang, J. Feng, M.L. Zhang, Mater. Res. Bull. 43 (2008) 3221–3226.
[18] H.X. Zhang, M.L. Zhang, Mater. Chem. Phys. 108 (2008) 184–187.
[19] D.P. Dubal, D.S. Dhawale, R.R. Salunkhe, V.S. Jamdade, C.D. Lokhande, J. Alloys Compd. 492 (2010) 26–30.
[20] K.P.S. Prasad, D.S. Dhawale, T. Sivakumar, S.S. Aldeyab, J.S.M. Zaidi, K. Ariga, A. Vinu, Sci. Technol. Adv. Mater. 12 (2011) 044602.
[21] S. Huang, G.N. Zhu, C. Zhang, W.W. Tjiu, Y.Y. Xia, T.X. Liu, ACS Appl. Mater. Interfaces 4 (2012) 2242–2249.
[22] S.R. Hwang, H.S. Teng, J. Electrochem. Soc. 149 (2002) A591–A596.
[23] Q.H. Men, L. Liu, H.H. Song, J. Appl. Electrochem. 36 (2006) 63–67.
[24] S.L. Candelaria, B.B. Garcia, D.W. Liu, G.Z. Cao, J. Mater. Chem. 22 (2012) 9884–9889.
[25] Y.J. Mai, X.L. Wang, J.Y. Xiang, Y.Q. Qiao, D. Zhang, C.D. Gu, J.P. Tu, Electrochim. Acta 56 (2011) 2306–2311.
[26] L. Vitos, A.V. Ruban, H.L. Skriver, J. Kollár, Surf. Sci. 411 (1998) 186–202.
[27] L.L. Zhang, J.Q. Liu, C. Tang, J.S. Lv, H. Zhong, Y.J. Zhao, X. Wang, Appl. Clay Sci. 51 (2011) 68–73.
[28] S.K. Meher, R.G. Rao, J. Power Source 215 (2012) 317–328.